

Article

Simple and Easily Connectable Transition from Empty Substrate-Integrated Waveguide to a 3D Printed Rectangular Waveguide

Darío Herraiz ^{1,*}, Angel Belenguer ¹, Marcos Fernandez ¹, Santiago Cogollos ², Héctor Esteban ²
and Vicente E. Boria ²

¹ Departamento de Ingeniería Eléctrica, Electrónica, Automática y Comunicaciones, Escuela Politécnica de Cuenca, Universidad de Castilla-La Mancha, Campus Universitario, 16071 Cuenca, Spain; angel.belenguer@uclm.es (A.B.); marcos.fernandez@uclm.es (M.F.)

² Instituto de Telecomunicaciones y Aplicaciones Multimedia, Universitat Politècnica de València, 46022 Valencia, Spain; sancobo@dcom.upv.es (S.C.); hesteban@upv.es (H.E.); vboria@dcom.upv.es (V.E.B.)

* Correspondence: dario.herraiztirado@uclm.es

Featured Application: The proposed transition enables the integration of 3D printing structures and SIC, particularly an ESIW guide, allowing for the combination of both technologies and manufacturing methods. As a result of this new transition, a wide range of diverse devices can be produced, offering affordability, simplicity, and excellent outcomes.

Abstract: 3D printing is one of the most promising manufacturing methods in the most developed technological fields, including microwave hardware fabrication. On the other hand, the well-known manufacturing methods of planar substrate integrated circuits allow high-quality prototypes to be made at low cost and with mass production capabilities. The combination of both manufacturing methods, 2D or 2.5D (substrate integrated circuits) and 3D (3D printed structures), will allow us to take advantage of the main strengths of each technology and minimise disadvantages. In this article, for the first time, a transition structure between the Empty Substrate-Integrated Waveguide (ESIW) technology—a planar waveguide integrated on a printed circuit board—and a standard rectangular waveguide manufactured by 3D printing is proposed. This transition will make it possible to combine planar circuits with 3D structures, thus taking advantage of the benefits of both types of technologies. The fabricated prototype presents low losses (0.6 dB for the transmission coefficient and 15 dB for reflection coefficient), good electrical response (very flat), and simultaneously good mechanical stability and robustness to manufacturing and assembly errors. The proposed design for this transition piece is easily realisable for a wide range of affordable 3D printers. Repeatability is guaranteed and the proposed transition allows us to combine different SIC structures to 3D printed circuits. Hence, this transition will enable advancements in the fabrication of microwave devices, particularly with regard to satellite communications.

Keywords: transition; planar circuits; waveguide technology; 3D printing; empty substrate integrated waveguide (ESIW); junction; substrate integrated circuits (SICs)



Citation: Herraiz, D.; Belenguer, A.; Fernandez, M.; Cogollos, S.; Esteban, H.; Boria, V.E. Simple and Easily Connectable Transition from Empty Substrate-Integrated Waveguide to a 3D Printed Rectangular Waveguide. *Appl. Sci.* **2023**, *13*, 11698. <https://doi.org/10.3390/app132111698>

Academic Editor: Lamberto Tronchin

Received: 6 October 2023

Revised: 20 October 2023

Accepted: 24 October 2023

Published: 26 October 2023



Copyright: © 2023 by the authors. Licensee MDPI, Basel, Switzerland. This article is an open access article distributed under the terms and conditions of the Creative Commons Attribution (CC BY) license (<https://creativecommons.org/licenses/by/4.0/>).

1. Introduction

The first ESIW (Empty Substrate-Integrated Waveguide) was introduced in 2014 [1]. Later, the first Air-Filled Empty Substrate Integrated Waveguide (AFSIW) was also proposed [2]. Since then, many passive devices have been implemented using these Substrate Integrated Circuit (SIC) technologies due to their main features: low losses, good electrical responses, compactness (footprint and volume reduction), and easy manufacturing. Similarly, since the arrival of 3D printing, many microwave devices and structures have been manufactured using some of the available 3D manufacturing techniques: FDM

(Fused Deposition Modeling), SLA (Stereolithography), and SLS (Selective Laser Sintering), among many others [3]. So far, the main applications of 3D printing in microwaves have been focused on implementing flanges and launchers, with very stringent manufacturing requirements [4,5]. Also, there have been some research studies on 3D manufacturing components for SIWs [6–8], but not for ESIW or transitions that connect them to other technologies, although this type of transition exists for other technologies [9]. Several previous attempts at approximating planar-to-3D transitions, as documented in references [10,11], have shown very limited versatility, very low bandwidth, and often exhibit complexity and high manufacturing costs. As both SICs and 3D printing techniques continue to advance and mature, a method for merging both of them and assembling devices of both types will be necessary to take advantage of the benefits of both technologies. In this article, the first transition from ESIW to a rectangular waveguide manufactured with 3D printing is presented. Therefore, it is for this reason that this transition will ease improvements in the interconnectivity and interoperability among microwave satellite circuits, with a specific emphasis on satellite communications, as elucidated in this article.

As discussed in [12], ESIW circuits are waveguides with discrete heights. Therefore, the transition between the ESIW lines and printed 3D waveguide does not require any type of adaptation circuit. In this particular case, the ESIW and the printed 3D waveguide are exactly the same waveguide (a and b are identical), and both of them are empty, so ϵ_R is the same. Thus, the main challenge when implementing this type of transition is to ensure good electrical contact between the planar circuitry and 3D structure. In this proposal, electrical continuity is guaranteed through tin soldering. The proposed transition is easy to solder, which guarantees good electrical continuity and, therefore, a good electrical response. With a transition in these characteristics, a new range of possibilities opens up that will allow us to design more advanced devices by exploiting the benefits of both technologies (SIW [13] and 3D printed waveguides), while reducing their corresponding weak points. The proposed transition in this article has been designed and experimentally validated for the Ku-band frequency range [14]. The 3D part has been manufactured using copper with a 3D printer using BDM (Bound Metal Deposition) technology.

2. Structure

The transition from ESIW to a rectangular waveguide is relatively simple from the electromagnetic point of view, since the ESIW itself is a rectangular waveguide of reduced height. Therefore, the main challenge in the transition proposed is not the matching of the original propagation mode to that of the new structure (which in this case coincides), but to ensure that the transition fully allows its propagation and transmission to take place with the lowest possible insertion and reflection losses. The coupling between the two rectangular waveguides—the planar waveguide (ESIW) and the 3D waveguide—will be improved as the electrical contact in the long walls of both waveguides is optimised, since in those walls the current changes direction constantly. Conversely, a lack of continuity in the short walls would not impact the transmission of the fundamental mode because the current along those walls is orthogonal to the propagation direction, making the connection between those short walls less critical. On the other hand, it is essential to ensure precise alignment of the waveguides, as small misalignments can result in unwanted reflections. To summarise, the proposed 3D structure must ensure accurate alignment of the waveguides when assembled with the planar circuitry, and provide physical access to the long walls of both waveguides to allow tin soldering in order to ensure a very good electrical continuity. As previously indicated [12], systems such as ESIW and waveguides belong to the same category of transmission systems, obviating the requirement for signal adaptation between them and phase discontinuities. Hence, with assured electrical continuity, the transitional performance is expected to be satisfactory, as we can see in the simulation shown in Figure 1. Furthermore, the welding must exhibit sufficient strength to forestall detachment of the device from the remainder of the structure. In this study, the primary focus has been on ensuring the feasibility of the transition in its simplest form. For future work, possibilities

for weight reduction, volume minimisation, design simplification, and other aspects may be explored. These objectives extend beyond the scope of this prototype and are going to be explored once this prototype has been validated.

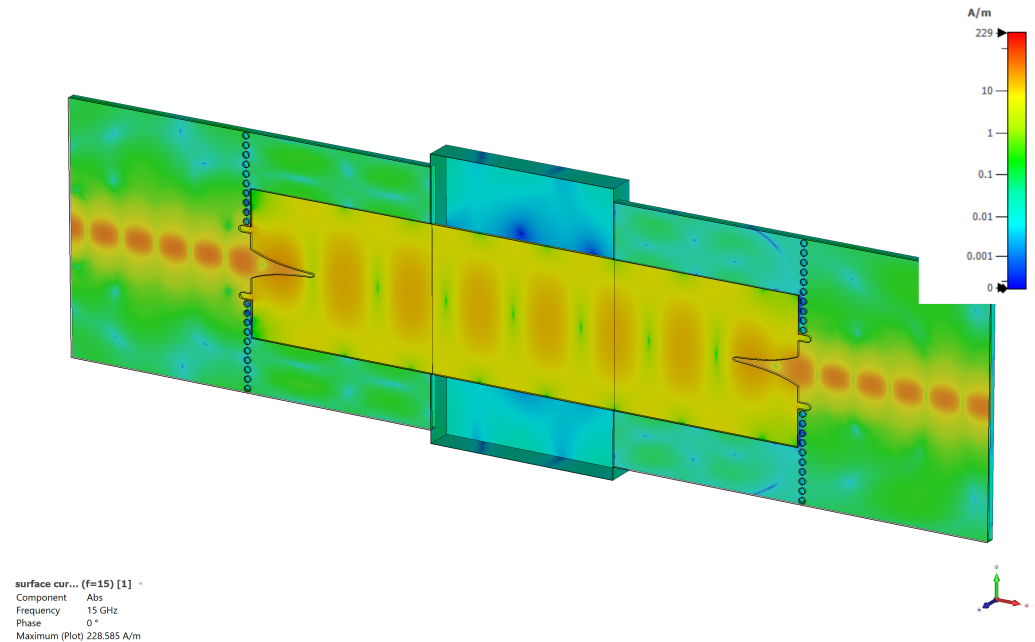


Figure 1. Electromagnetic propagation in the lines across the transition.

2.1. Requirements

The 3D waveguide must ensure two essential aspects as shown before:

1. Precise alignment: The 3D waveguide must guarantee a precise alignment with the planar waveguide (ESIW) to avoid deviations and unwanted reflections.
2. Adequate electrical connection with the ESIW feed: to maintain the electric field confined within the waveguide and avoid mismatches and reflections.

2.2. Development of the Junction

Based on the above-mentioned ideas, four different structures for the transition are initially proposed, which can be seen in Figure 2.

- Full robust structure: good mechanical fit, but poor soldering due to the difficulty of the soldering paste to flow into the gap, Figure 2a.
- Structure with U-shaped aligning elements: easy welding and sufficient mechanical adjustment. Once soldered, the prototype is very robust thanks to the U-shaped elements and the welding, Figure 2b.
- Dowel pins as aligning elements: very easy welding and sufficient mechanical adjustment with dowel pins. Using external elements, precision does not depend on the resolution of the printer and precision rises. Because of the sintering process [15] used to build the 3D part, deformations are higher than expected due to the circular geometry for the dowel pins. Because of that, results are not that good but still good enough. It is necessary to clarify that other 3D printing technologies do not depend on the sintering process, which is why these results are included, Figure 2c.
- Substrate fragments as aligning elements: very easy welding and sufficient mechanical adjustment with substrate fragments. Using external elements, precision does not depend on the resolution of the printer and precision rises, Figure 2d.

With a completely solid structure like the one shown in Figure 2a, it may appear initially that the aforementioned requirements are better met. However, if the transition is manufactured in this way, it will not be possible to directly access the contact zone between

the long walls of both waveguides, making it impossible to achieve good electrical contact between them, as there is no way to ensure that the tin will penetrate enough into the structure. Therefore, this structure (Figure 2a) was discarded in this work once fabricated and measured in order to prove the above statement and the results of the measured prototype evidence this. The U-shaped alignment elements, dowel pins, and substrate fragments were selected because they ensure adequate mechanical fit and the connection between the waveguides is fully accessible for performing the necessary soldering. For the soldering to be effective, which is crucial for the operation of the transition, it is important that the edges around the end of the feeding ESIW waveguides that face the 3D waveguide are fully metallised, as shown in Figure 3. Based on the manufactured and measured devices, it has been ascertained that the device exhibits a notably high level of mechanical resistance, largely attributed to the quality of soldering. As such, this particular component does not pose any concerns in any conceivable scenario. The soldering integrity surpasses that of the ESIW circuit, positioning the power circuit as the primary vulnerability. Furthermore, in the specific context of the U-shaped alignment structures, their robustness is even more pronounced.

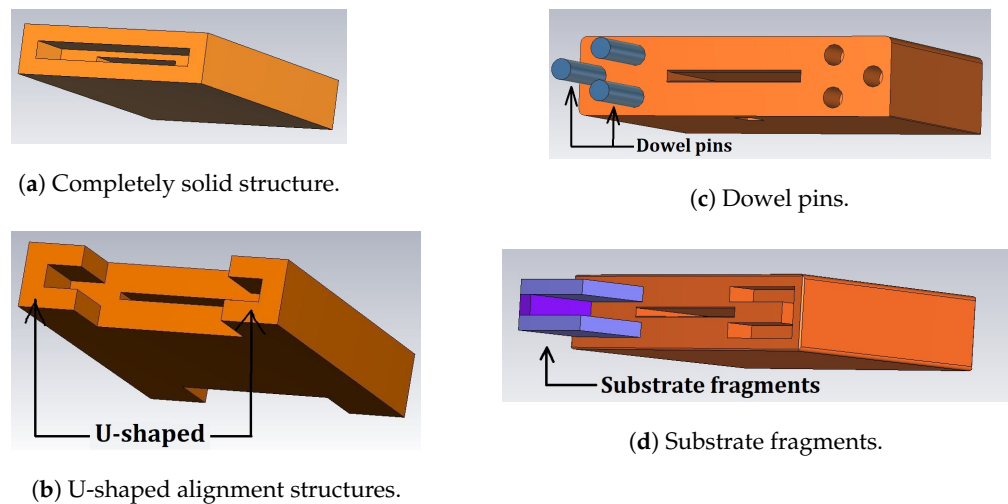


Figure 2. Development of the proposed transition.

To validate the transition experimentally, a back-to-back prototype of the proposed device was manufactured. The prototype was fed with microstrip lines that will connect it to the Vector Network Analyzer (VNA) for its characterisation. To complete the back-to-back prototype, two microstrip-to-ESIW transitions were added to both the input and output ports. Finally, the prototype was completed with two twin versions of the ESIW-to-3D waveguide transition (see Figure 3), which is what we intend to validate in this work. Figure 4 depicts the structure of the back-to-back prototype used to validate the proposed transition, with the top covers of the feed ESIWs omitted to show all elements in detail. The performance of the back-to-back transition was initially validated through simulations, which were also used to assess the resilience of the proposed solution against possible manufacturing inaccuracies.

All the simulations were carried out with the full-wave simulator CST Studio Suite v21. Hereinafter, the metal piece will be referred to as a 3D guide, and the feed circuits as ESIW circuits.

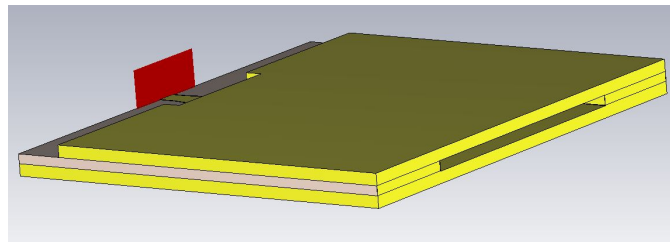


Figure 3. Feeding line: a 3-layer ESIW prototype ended in an open waveguide with metallised faces. Yellow material is copper and light brown is Rogers 4003C.

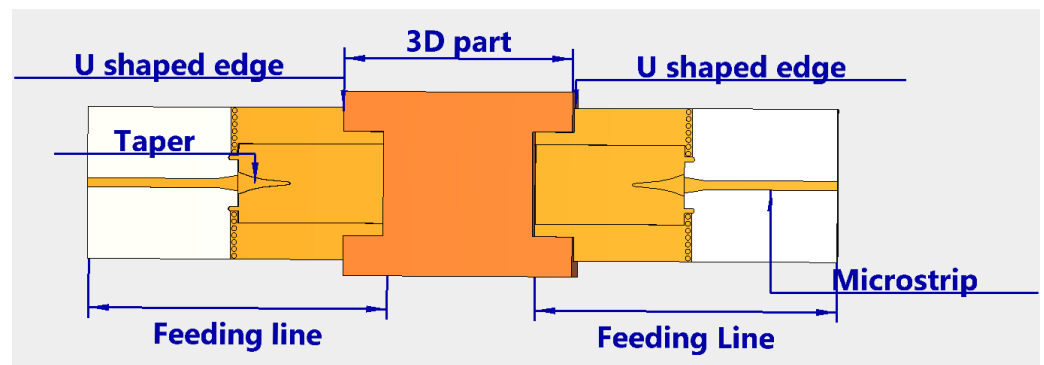


Figure 4. Development of the transition.

3. Assembling Procedure

The assembly between the ESIW circuits and the 3D guide must be achieved following this procedure:

1. Sand the faces of the 3D guide that will be soldered with the ESIW circuits. By sanding these surfaces, irregularities are reduced, allowing a better welding.
2. Align the ESIW circuits with the 3D guide using the alignment axes or external elements for dowel pins and substrates fragments as alignment elements. These should be tightened as much as possible to minimise the gap between the components.
3. Apply solder paste to the joint area of the 3D guide and the ESIW circuits, and heat with a soldering iron unit (welder) until it melts. The adjustment should be made before the application of the solder paste to prevent tin from leaking inside the guide.
4. Wait for the soldering paste to cool.
5. Repeat for the other feed line.

It is critical that connectivity between successive components is guaranteed. To prevent solder paste from seeping into the cavity, thus worsening the response, vertical welding orientation is recommended. Otherwise, it would not be possible to insert the ESIW circuit. To reduce manufacturing errors, it is advisable to minimise this gap as much as possible within the constraints of the 3D printing system used.

4. Error Sources

To study the robustness and error tolerance of the proposed device, several simulations have been carried out. The main area where sources of errors that can be corrected have been detected is in the assembly zone between the 3D guide and power lines. Errors are drastically reduced by minimising the inevitable assembly gap, as previously mentioned. In Table 1, all identified error sources are summarised.

Table 1. Table of summarised error sources.

Source	Effect	Importance
Mismatching	Losses	Low
Rotation	Losses and frequency resonance peaks	High
Tin pouring	Losses	Low
Deformations	Unpredictable	Unpredictable
Combination	Unpredictable	High

4.1. Mismatching Connections

When welding the different parts of the circuit, it is very complex to perfectly align ESIW circuits with the 3D guide, as shown in Figure 5. This displacement between the guides is not very critical, the device is quite robust to these displacements; in fact, considering slight movements of 50 μm in both axes (X and Y), the losses are below 1 dB throughout the working band.

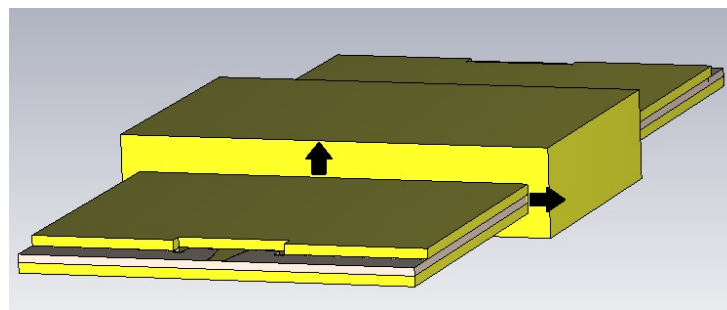
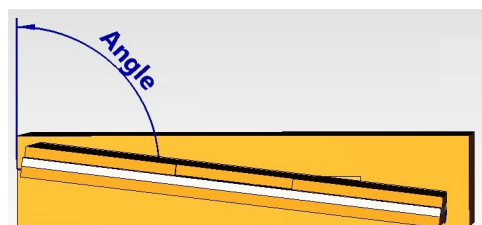


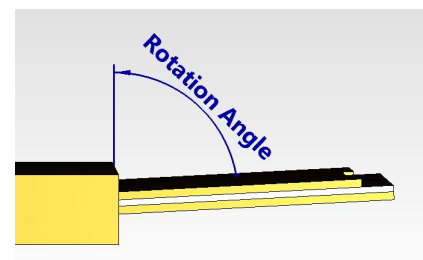
Figure 5. Mismatch between the feeding line and the printed part. The alignment U-shaped structures have been omitted in this picture in order to show this effect better. Black arrows show the directions of the displacement.

4.2. Rotation

This effect is the most critical one. The performance of the device degrades rapidly as the angle of the power lines increases with respect to the 3D guide. The rotation affects all axes, as shown in Figure 6. This effect can be explained by the electric field polarisation; a small angle forces the electric field to change direction in order to propagate. The rotation effect of both power lines with respect to the 3D guide shows losses below 1 dB for angles with values below 1.9° . Significant rotation angles produce different resonance peaks displaced in frequency, and with different amplitude values depending on the particular angle value.



(a) Rotation in X–Y plane (angles can be different in each side of both feeding lines).



(b) Rotation angle in Y–Z plane.

Figure 6. Rotation error. The alignment axes have been omitted in this picture in order to show this effect better.

4.3. Welding Effect–Tin Pouring

When welding, the solder paste used to join the feed lines and the 3D guide may partially seep inside or not seep at all, and depending on the gap between them, the amount of tin seeped inside will be higher or lesser (see Figure 7). This results in slight losses depending on the amount of tin that has seeped in (see Figures 8 and 9). If the adjustment between the power lines and the 3D guide is well done, the effect produced by the small gap is completely negligible.

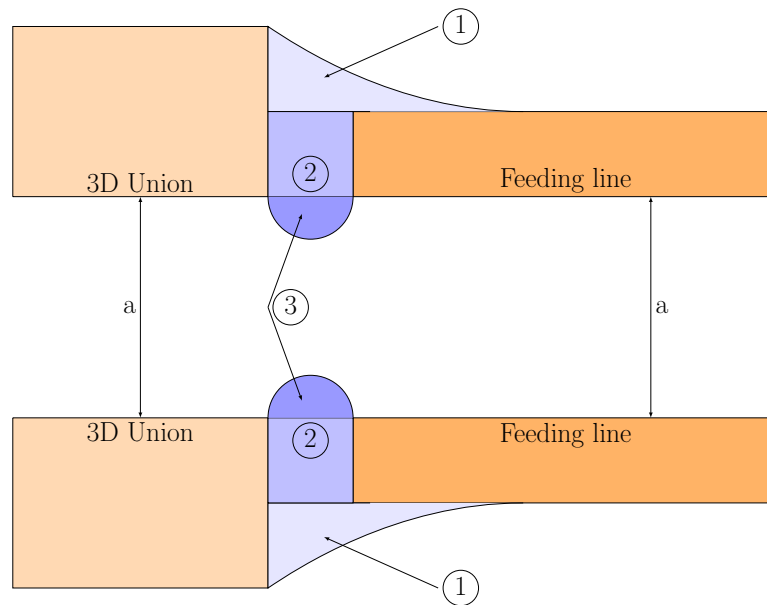


Figure 7. Sectional view of overflowing tin. Tin (purple) pours inside the gap between the junction and the feeding lines, it penetrates a greater or a lesser amount in the gap. Three different cases have been considered: (1) soldering paste does not pour inside (*nopour*), (2) soldering paste pours a bit (*perfect*), and (3) soldering paste pours inside the waveguide (*pour*). The alignment axes have been omitted in this picture in order to show this effect better.

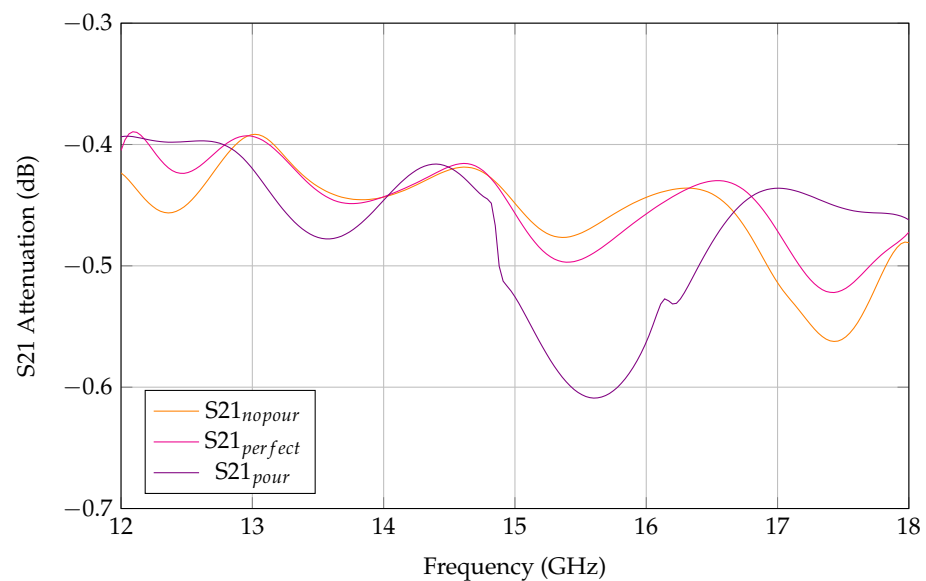


Figure 8. Soldering paste effect (S21): no pour, perfect, and pour.

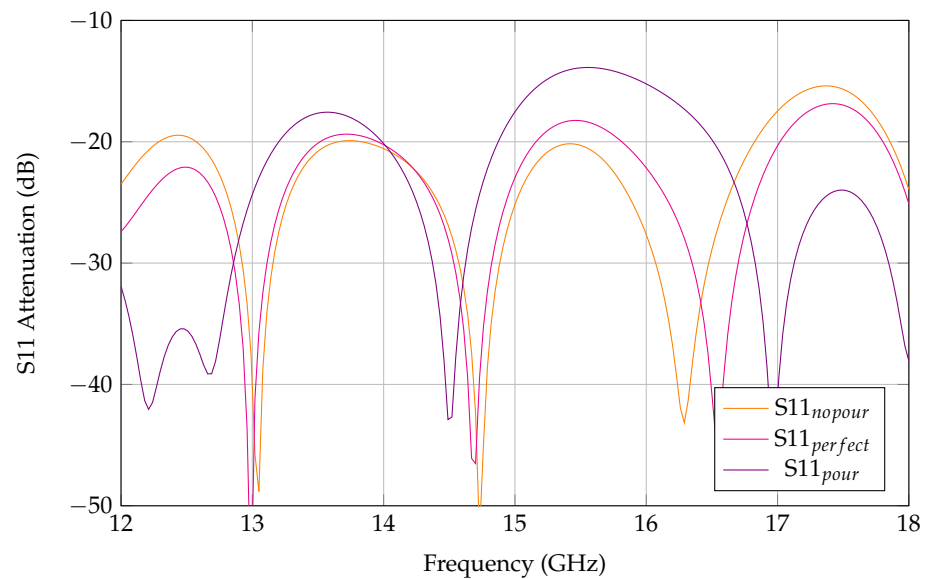


Figure 9. Soldering paste effect (S11): no pour, perfect, and pour.

4.4. Deformations due to 3D Printing

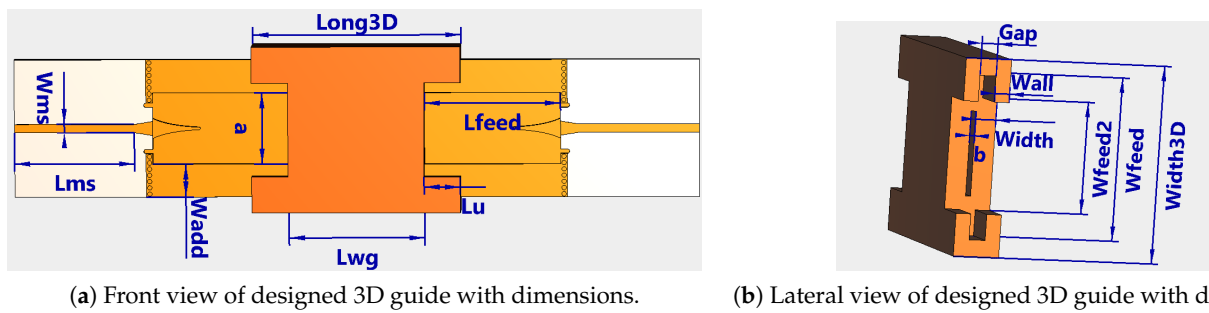
Depending on the technology used to print the 3D guide, the piece will suffer deformations, bends, and other negative effects. For instance, the sintering process [15] is required for the manufacture of this prototype. This process heats the part to very high temperatures, causing it to compress and deform (which can be partially compensated), as well as other possible undesired effects.

4.5. Combination of Different Errors

Individually, each error has a limited impact on the prototype behaviour. However, the combination of these errors can degrade its performance significantly. Therefore, it is crucial to design an alignment system that fit the power lines and the 3D guide as precisely as possible. By minimising these errors, most of the previously mentioned degradations will be reduced, excluding those caused by unpredictable deformations in the 3D guide.

5. Discussion

A back-to-back prototype for Ku-band has been manufactured. The metal piece has been printed using high purity copper (99.9%) and the power lines have been manufactured with Rogers 4003C for the central layer and FR-4 for the covers. All the involved geometrical parameters are collected in Table 2, and their meaning can be seen in Figure 10. The parameters a and b are determined by the ESIW guide, and Gap depends on the total height of the power circuits. The parameter L_{ms} does not impact the behaviour of the transition, so this length can have any value. In this case, the length chosen matches with the length of the calibration kit used to discount the effect of the microstrip lines on the measurements. W_{ms} is determined by the selected input impedance, the operating frequency, and the substrate used to manufacture the microstrip line. The rest of the parameters do not affect the electrical response of the prototype and can be freely chosen in order to optimise manufacturing time, reduce the amount of material used, provide greater robustness, etc.



(a) Front view of designed 3D guide with dimensions.

(b) Lateral view of designed 3D guide with dimensions.

Figure 10. Geometrical dimensions of the prototype.**Table 2.** Table of geometrical parameters.

Parameter	Value	Parameter	Value
a	15.7988 mm	Width _{3D}	36.71 mm
b	0.966 mm	Long _{3D}	46 mm
L _{wg}	20 mm	Width	3.85 mm
L _{feed}	25 mm	Gap	3.07 mm
L _{ms}	25 mm	Wall	2.8 mm
W _{ms}	1.82 mm	W _{feed}	30.40 mm
W _{add}	7.29 mm	W _{feed2}	20.80 mm
L _u	8 mm		

Figures 11 and 12 show four different responses: the ideal back-to-back simulation (*Ideal*) and the three different responses of the fabricated devices with the different aligning elements (*pins*, *substrate*, and *u-shaped*). The prototype has been measured with the Anritsu MS4644A 2-port Vector Network Analyzer (VNA) and calibrated with a custom TRL (thru-reflect-line) microstrip calibration kit. This kit is designed for the Ku-band and the substrate used for both ESIW circuit central layers. This calibration moves the reference measurement plane to the beginning of the microstrip-to-ESIW transition, avoiding the losses introduced by the microstrip lines and the coaxial connector. Therefore, the measurements will show the back-to-back response of the microstrip-to-ESIW transition and the ESIW-to-3D guide transition (which is what is really intended to be evaluated). Consequently, the measured results will always be worse than those of the ESIW-to-3D guide transition alone. The observed degradation both in the simulated and measured responses is mainly due to the non-ideal response of the microstrip-to-ESIW transitions, which had to be included in order to measure with the VNA, and could not be eliminated with the calibration kit. As shown in Figures 11 and 12, in the worst-case scenario, losses do not exceed 1 dB for substrate and U-shaped aligning elements and around 1.5 dB for dowel pins, while in the best-case scenario they approach 0.4 dB. This response is relatively flat, and losses increase as the frequency rises, which is a typical characteristic of most manufactured prototypes. The reflection coefficient is almost always below -15 dB. The discrepancies between the measured and simulated results are considered to be minimal. As a result, the proposed fabrication and soldering method delivers a response that is very close to the ideal simulation case, thereby confirming the validity of the proposed transition and its manufacturing process.

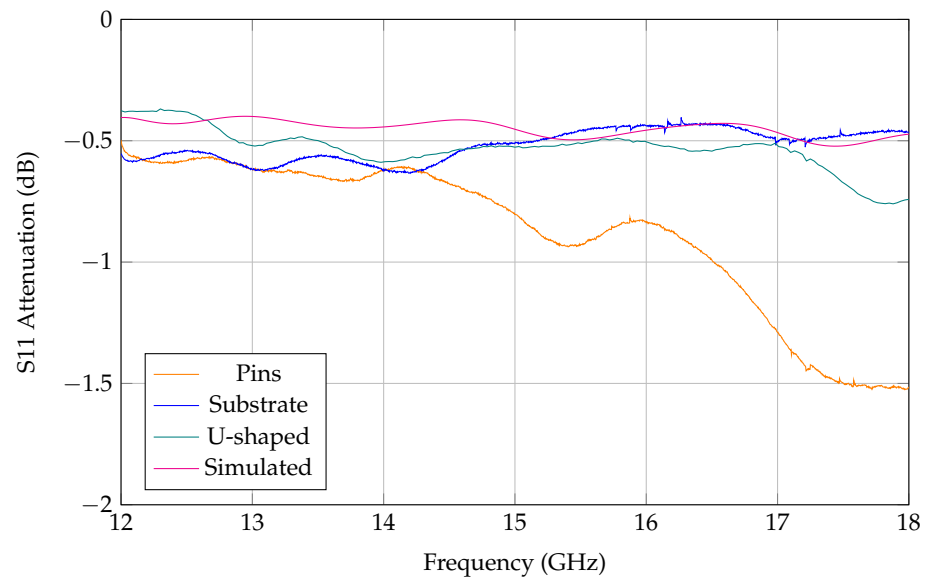


Figure 11. Transmission coefficient (S₁₁) of various structures of SIW-to-3D waveguide transition: pins, substrate, u-shaped, and ideal.

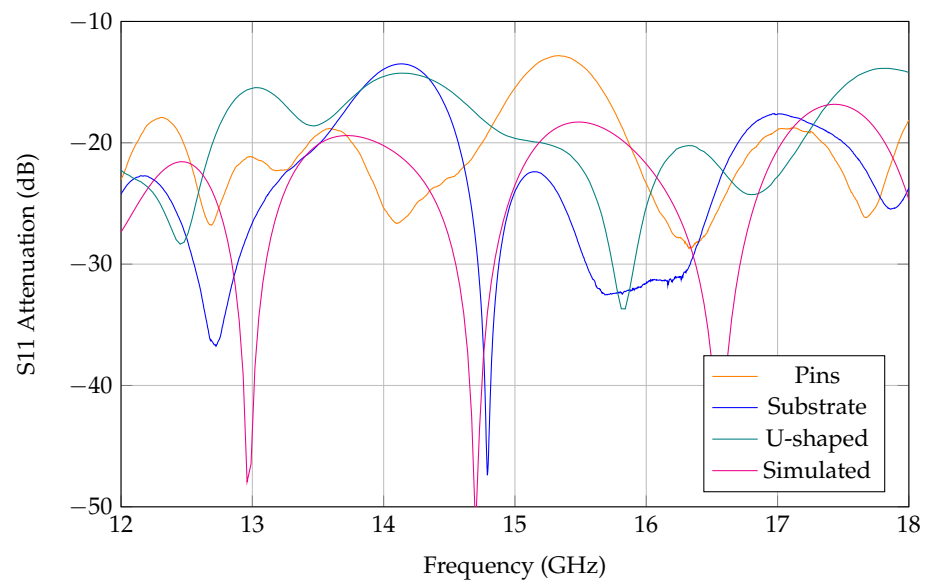
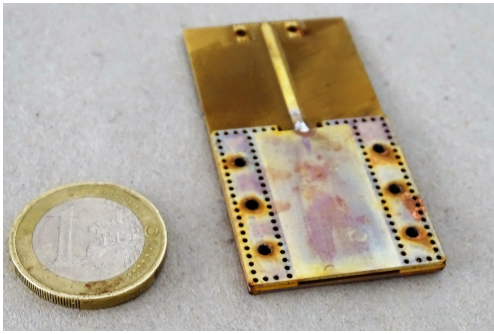
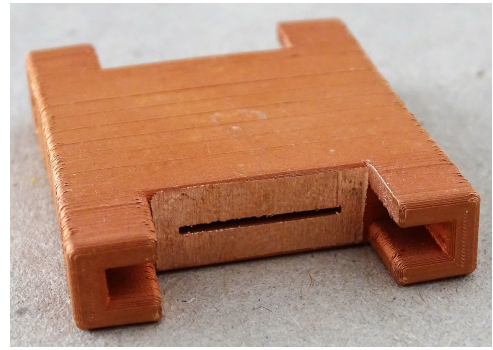


Figure 12. Transmission coefficient (S₁₁) of various structures of SIW-to-3D waveguide transition: pins, substrate, u-shaped, and ideal.

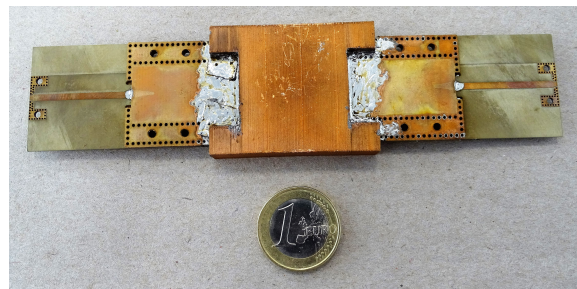
The final prototype and its parts can be seen in Figure 13. The device functions correctly and can be utilised to integrate 3D components with planar circuits, such as filters and antennas. The 3D guide has been fabricated in copper, although other alternatives could be considered to reduce costs or minimise losses. For example, the 3D parts could be manufactured in cheaper polymers or metals, and then metallised afterwards with a good conductor layer. Manufacture characteristics of the 3D printed part can be seen in Figure 14. Thanks to the ESIW-to-3D waveguide transition presented in this article, some of the transition from planar lines to ESIW [16–18] can be used to connect these planar lines to 3D structures, such as 3D printed antennas [19], without the need of flanges, and with a good electrical performance. It allows us also to connect with different Ridge waveguides devices (antennas, dividers, etc.) [20–25]. Additionally, this device can benefit from both manufacturing techniques SIC [26] and additive manufacturing [27,28].



(a) Feed line. Some fencing vias have been added in order to avoid metallisation problems inside the waveguide.



(b) Printed part.



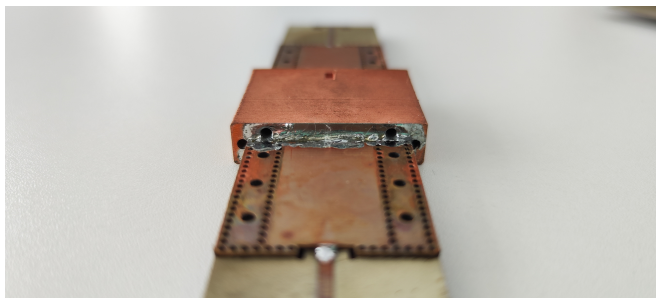
(c) Full assembled prototype with removable connectors.



(d) Printed part (Dowell pins).



(e) Printed part (Substrate).



(f) Printed part Dowell pins detail.



(g) Printed part substrate detail.

Figure 13. Parts of the prototype and integrated structure.

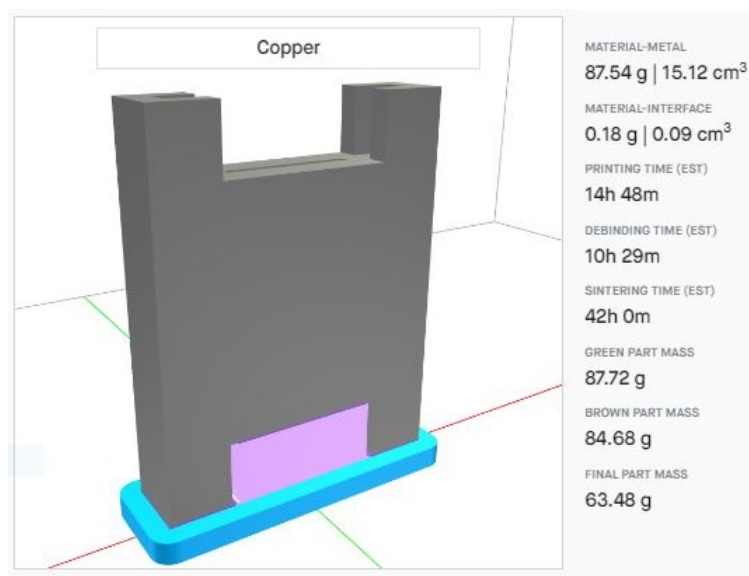


Figure 14. Manufacturing characteristics of the 3D part. The estimated cost of copper is USD 16.23.

The comparison with other transitions can be observed in Table 3, noting that the compared devices are quite different from the one proposed in this article since it is the first of its kind. Therefore, this comparison serves more as an overview of current transitions. The proposed transition is easy to manufacture and design, works with very low losses in the operation bandwidth, and connects two technologies that could not be connected easily until now. As we can observe, the proposed transition exhibits very minimal losses. In fact, it stands as the best in terms of losses. Furthermore, it seamlessly adapts to other frequencies by adjusting the values of *a* and *b* without the need for optimisation, in contrast to the other ones. In terms of bandwidth, it perfectly covers the entire bandwidth of the WR-62 standard for waveguides, and if necessary, it is possible to cover very wide frequency bands, for example by incorporating the ridge section.

Table 3. Comparison performance with other transitions.

Ref.	Figure of Merit	Frequency Band	Transition	Complexity
[9]	$T_1 = 250 \mu\text{s}$, $Q_i = 11.2 \cdot 10^6 \text{ dB}$	3–17 GHz	Stripline-3D cQED	High
[29]	$I_L \text{ (dB)} = 0.83 \text{ dB}$, $R_L = 21 \text{ dB}$	26–40 GHz	MS-ESIW	Medium
[5]	$I_L \text{ (dB)} = 2 \text{ dB}$, $R_L = 8 \text{ dB}$	X (8–12 GHz)	MPRWG-DiRWG	Very High
[10]	$I_L \text{ (dB)} = 0.95 \text{ dB}$, $R_L = 15 \text{ dB}$	33–36.7 GHz	SIW-Rectangular Waveguide	Very High
This work	$I_L \text{ (dB)} = 0.6 \text{ dB}$, $R_L = 15 \text{ dB}$	K_u (12–18 GHz)	ESIW-3D	Low

6. Conclusions

The device presented in this article exhibits strong performance as a transitional component from planar technology to 3D-printed components. It demonstrates minimal signal losses, typically below 1 dB, even when considering the introduction of microstrip-to-ESIW transitions, which were incorporated solely for the purpose of VNA measurements. The device’s ease of fabrication and assembly, coupled with its potential for fostering the development of fully integrated 3D structures and planar circuits, enables the seamless integration of SIC technologies with 3D printed components. Furthermore, its resilience against manufacturing errors and compatibility with a range of readily available, cost-effective 3D printers ensures repeatability. This method can also be applied to waveguide sizes across various frequency ranges. Moreover, the robustness of the soldering process prevents deformation or detachment of the device post-soldering. In the context of future advancements, this prototype serves as a foundational platform for creating more intricate

devices and geometries previously considered unattainable using SIC manufacturing techniques. This will enable smaller-scale laboratories to manufacture these devices without the need to invest in expensive fabrication equipment or similarly costly high-performance devices. Examples of such prototypes encompass high-quality filters, dividers, couplers, and horn antennas, to name a few. While the current device boasts robustness, it remains a compelling avenue for future research to subject the device to thermal and mechanical stress conditions to further its characterisation, as well as some other improvements that are going to be considered once this prototype has been validated.

Author Contributions: Conceptualization, D.H., A.B., M.F., S.C., H.E. and V.E.B.; methodology, D.H. and A.B.; software, D.H. and A.B.; validation, D.H.; formal analysis, D.H.; investigation, D.H.; resources, D.H. and A.B.; data curation, D.H. and S.C.; writing—original draft preparation, D.H. and M.F.; writing—review and editing, D.H., A.B., M.F., S.C., H.E. and V.E.B.; supervision, A.B., M.F., H.E.; project administration, A.B. and V.E.B.; funding acquisition, A.B. and V.E.B. All authors have read and agreed to the published version of the manuscript.

Funding: This research was funded by the Ministerio de Ciencia e Innovación, Spanish Government, and the European Union NextGenerationEU/PRTR, through the Subprojects C44 and C41 of the Coordinated Project TED2021-129196B, under Grant MCIN/AEI/10.13039/501100011033. This work has been financed by European Social Fund + (ESF+).

Institutional Review Board Statement: Not applicable.

Informed Consent Statement: Not applicable.

Data Availability Statement: Data sharing not applicable.

Conflicts of Interest: The authors declare no conflict of interest.

Abbreviations

SIC	Substrate Integrated Circuit
SIW	Substrate Integrated Waveguide
ESIW	Empty Substrate Integrated Waveguide

References

1. Belenguer, A.; Esteban, H.; Boria, V. Novel empty substrate integrated waveguide for high-performance microwave integrated circuits. *IEEE Trans. Microw. Theory Tech.* **2014**, *62*, 832–839. Available online: <https://ieeexplore.ieee.org/document/6766283> (accessed on 23 October 2023). [CrossRef]
2. Ranjkesh, N.; Shahabadi, M. Reduction of dielectric losses in substrate integrated waveguide. *Electron. Lett.* **2006**, *42*, 1230–1231. [CrossRef]
3. Booth, P.A.; Lluch, E.V. Realising advanced waveguide bandpass filters using additive manufacturing. *IET Microwaves, Antennas Propag.* **2017**, *11*, 1919–2108. [CrossRef]
4. Delmonte, N.; Silvestri, L.; Tomassoni, C.; Piekarz, I.; Sorocki, J.; Perregri, L.; Bozzi, M. Design and manufacturing of microwave components by 3D printing. In Proceedings of the 2022 Microwave Mediterranean Symposium (MMS), Pizzo Calabro, Italy, 9–13 May 2022. [CrossRef]
5. D’Auria, M.; Otter, M.D.W.J.; Hazell, J.; Gillatt, B.T.W.; Long-Collins, C.; Ridler, N.M.; Lucyszyn, S. 3-D printed metal-pipe rectangular waveguides. *IEEE Trans. Components, Packag. Manuf. Technol.* **2015**, *5*, 1339–1349. [CrossRef]
6. Moscato, S.; Bahr, R.; Le, T.; Pasian, M.; Bozzi, M.; Perregri, L.; Tentzeris, M.M. Additive manufacturing of 3D substrate integrated waveguide components. *Electron. Lett.* **2015**, *51*, 1426–1428. [CrossRef]
7. Moro, R.; Bozzi, M.; Collado, A.; Georgiadis, A.; Via, S. Plastic-based Substrate Integrated Waveguide (SIW) components and antennas. In Proceedings of the 2012 42nd European Microwave Conference, Amsterdam, The Netherlands, 29 October–1 November 2012; pp. 1007–1010. [CrossRef]
8. MacDonald, E.; Salas, M.R.; Espalin, D.; Perez, M.; Aguilera, E.; Muse, D.; Wicker, R.B. 3D Printing for the Rapid Prototyping of Structural Electronics. *IEEE Access* **2014**, *2*, 234–242. [CrossRef]
9. Axline, C.; Reagor, M.; Heeres, R.; Reinhold, P.; Wang, C.; Shain, K.; Pfaff, W.; Chu, Y.; Frunzio, L.; Schoelkopf, R.J. An architecture for integrating planar and 3D cQED devices. *Appl. Phys. Lett.* **2016**, *109*, 042601. [CrossRef]
10. Dai, X. An Integrated Millimeter-Wave Broadband Microstrip-to-Waveguide Vertical Transition Suitable for Multilayer Planar Circuits. *IEEE Microw. Wirel. Components Lett.* **2016**, *26*, 897–899. [CrossRef]

11. Rida, A.; Margomenos, A.; Wu, T.; Tentzeris, M.M. Novel wideband 3D transitions on Liquid Crystal Polymer for millimeter-wave applications up to 100 GHz. In Proceedings of the 2009 IEEE MTT-S International Microwave Symposium Digest, Boston, MA, USA, 7–12 June 2009; pp. 953–956. [[CrossRef](#)]
12. Belenguer, A.; Fernandez, M.D.; Ballesteros, J.A.; Esteban, H.; Boria, V.E. Experimental study in Ku-band of the propagation inside Empty Substrate Integrated Waveguides. In Proceedings of the 2016 46th European Microwave Conference (EuMC), London, UK, 4–6 October 2016; pp. 639–642. [[CrossRef](#)]
13. Belenguer, A.; Esteban, H.; Borja, A.L.; Boria, V.E. Empty SIW technologies: A major step toward realizing low-cost and low-loss microwave circuits. *IEEE Microw. Mag.* **2019**, *20*, 24–45. [[CrossRef](#)]
14. Esteban, H.; Belenguer, A.; Sánchez, J.R.; Bachiller, C.; Boria, V.E. Improved low reflection transition from microstrip line to empty substrate-integrated waveguide. *IEEE Microw. Wirel. Components Lett.* **2017**, *27*, 685–687. [[CrossRef](#)]
15. Desktop Metal. Thermal Debinding and Sintering 101 | Desktop Metal. Available online: <https://www.desktopmetal.com/resources/sintering-101> (accessed on 23 October 2023).
16. Parment, F.; Ghiotto, A.; Vuong, T.-P.; Duchamp, J.-M.; Wu, K. Broadband transition from dielectric-filled to air-filled Substrate Integrated Waveguide for low loss and high power handling millimeter-wave Substrate Integrated Circuits. In Proceedings of the 2014 IEEE MTT-S International Microwave Symposium (IMS2014), Tampa, FL, USA, 1–6 June 2014; pp. 1–3. [[CrossRef](#)]
17. Peng, H.; Zhao, F.; Liu, Y.; Tatu, S.O.; Yang, T. Robust microstrip to empty substrate-integrated waveguide transition using tapered artificial dielectric slab matrix. *IEEE Microw. Wirel. Components Lett.* **2020**, *30*, 849–852. [[CrossRef](#)]
18. Peng, H.; Xia, X.; Dong, J.; Yang, T. An improved broadband transition between microstrip and empty substrate integrated waveguide. *Microw. Opt. Technol. Lett.* **2016**, *58*, 2227–2231. [[CrossRef](#)]
19. Yao, H.; Sharma, S.; Henderson, R.; Ashrafi, S.; MacFarlane, D. Ka band 3D printed horn antennas. In Proceedings of the 2017 Texas Symposium on Wireless and Microwave Circuits and Systems (WMCS), Waco, TX, USA, 30–31 March 2017; pp. 1–4. [[CrossRef](#)]
20. Wei, L.; XiaoLi, X. Design and Simulation of TEM Double Ridge Guide Horn Antenna. In Proceedings of the 2007 8th International Conference on Electronic Measurement and Instruments, Xi'an, China, 16–18 August 2007; pp. 1703–1706. [[CrossRef](#)]
21. Kazemi, R.; Fathy, A.E. Design of single-ridge SIW power dividers with over 75% bandwidth. In Proceedings of the 2014 IEEE MTT-S International Microwave Symposium (IMS2014), Tampa, FL, USA, 1–6 June 2014; pp. 1–3. [[CrossRef](#)]
22. Choudhury, S.; Mohan, A.; Mishra, P.K.; Guha, D. Wideband Pyramidal Ridged Horn Design by SIW Technology. *IEEE Antennas Wirel. Propag. Lett.* **2019**, *18*, 1517–1521. [[CrossRef](#)]
23. Romano, F.; Delmonte, N.; Tomassoni, C.; Perregrini, L.; Bozzi, M. 3D-Printed Compact Waveguide Filters Based on Slanted Ridge Resonators. In Proceedings of the 2022 IEEE/MTT-S International Microwave Symposium—IMS 2022, Denver, CO, USA, 19–24 June 2022; pp. 96–99. [[CrossRef](#)]
24. Mohammad-Ali-Nezhad, S.; Mallahzadeh, A. Periodic Ridged Leaky-Wave Antenna Design Based on SIW Technology. *IEEE Antennas Wirel. Propag. Lett.* **2015**, *14*, 354–357. [[CrossRef](#)]
25. Su, Y.; Lin, X.Q.; Fan, Y. Dual-polarized leaky wave antenna with low cross-polarization based on the mode composite ridged waveguide. In Proceedings of the 2020 International Conference on Microwave and Millimeter Wave Technology (ICMMT), Shanghai, China, 20–23 September 2020; pp. 1–3. [[CrossRef](#)]
26. Moscato, S.; Silvestri, L.; Delmonte, N.; Pasian, M.; Bozzi, M.; Perregrini, L. SIW components for the Internet of Things: Novel topologies, materials, and manufacturing techniques. In Proceedings of the 2016 IEEE Topical Conference on Wireless Sensors and Sensor Networks (WiSNet), Austin, TX, USA, 24–27 January 2016; pp. 78–80. [[CrossRef](#)]
27. Kaartinen, H.; Köyhäjoki, T.; Wenngren, J.; Bjork, E. Utilizing 3D printing in manufacturing companies: Comparative demonstration in a company case. In Proceedings of the 2018 2nd International Symposium on Small-scale Intelligent Manufacturing Systems (SIMS), Cavan, UK, 16–18 April 2018; pp. 1–4. [[CrossRef](#)]
28. Lindwall, A.; Dordlofva, C.; Öhrwall, A. Additive Manufacturing and the Product Development Process: Insights from the Space Industry. In Proceedings of the International Conference on Engineering Design (ICED17), Vancouver, BC, Canada, 21–25 August 2017; Volume 5.
29. Liu, Z.; Xu, J.; Wang, W. Wideband Transition From Microstrip Line-to- Empty Substrate-Integrated Waveguide Without Sharp Dielectric Taper. *IEEE Microw. Wirel. Components Lett.* **2019**, *29*, 20–22. [[CrossRef](#)]

Disclaimer/Publisher’s Note: The statements, opinions and data contained in all publications are solely those of the individual author(s) and contributor(s) and not of MDPI and/or the editor(s). MDPI and/or the editor(s) disclaim responsibility for any injury to people or property resulting from any ideas, methods, instructions or products referred to in the content.